The low-noise potential of low-vibration track

Jannik S. Theyssen, Astrid Pieringer, Wolfgang Kropp

Applied Acoustics, Chalmers University of Technology, Gothenburg, Sweden. Email: jannik.theyssen@chalmers.se

Introduction

Slab tracks systems, in which several concrete layers replace the traditional ballast and sleepers, are increasingly used on high-speed lines for their low maintenance and high tolerance [1]. For similar reasons, they are often found on bridges and in tunnels [2]. However, rolling on slab tracks often shows higher levels of noise compared to traditional track systems with ballast and sleepers. Two effects are contributing to this increase: The lack of the acoustic absorption of the ballast and the typically lower stiffness of the rail pads are main contributors to this increase [3, 2, 1]. The softer rail pads are necessary to control the total track stiffness, since the concrete panels provide a stiffer foundation compared to a system using ballast and sleepers. The consequence is a weaker coupling of the rail to the supporting structure and thus, more vibrational energy stays in the rail and eventually radiates into the surrounding air [4]. In other words, the decay of the vibration along the rail is low, which is typically described using the track decay rate (TDR) [5, 3].

Radiation from the track occurs via the ground as ground-borne vibration (perceivable vibrations), ground-borne noise (radiation from ground-borne vibrations) [6] or directly as air-borne noise. In the latter case, the sleepers, rails and wheels dominate the total noise in different frequency regions in the case of a ballasted track [3]. This is visualised in Figure 1. No large contribution

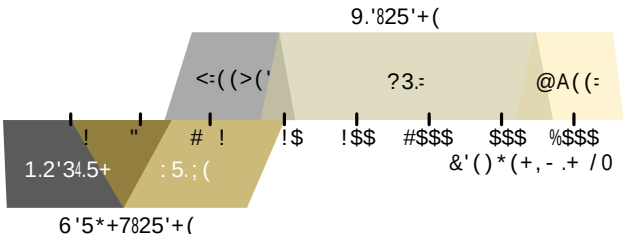

Figure 1: Dominant noise transfer path by frequency.

of the slab surface vibration to the airborne noise was found in [7].

Several different slab track systems exist. Often, the rail is directly attached to a concrete panel and so the rail pad needs to provide most of the necessary vertical flexibility. However, the low-vibration track (LVT), which is the focus in this work, provides a two-level elastic support. This system is depicted in Figure 2. Each of the two rails is supported by rail pads, which themselves rest on individual concrete blocks. The rubber boot around these concrete blocks provides an additional elasticity, in which an elastic inlay is placed for extra control of the vertical dynamic response of the stack. The concrete blocks are hereafter referred to as individually booted sleepers, however, they should not be confused with traditional, wide, monobloc sleepers that support both rails.

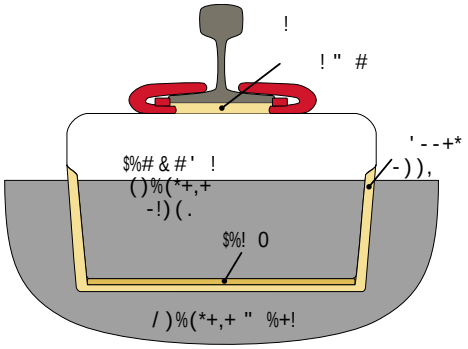

Figure 2: The (acoustically relevant) components of a slab track system with individual booted sleepers.

In this article, two configurations of the rail pad and inlay stiffness are compared for a unit force harmonic excitation. The first one, setup A, corresponds to the configuration currently used on tracks. In configuration B, the rail pad stiffness is significantly increased while the vertical boot elasticity is reduced by using a lower inlay stiffness. The TDRs of both configurations are compared. The goal of this article is to investigate if exchanging the rail pads and elastic inlays on existing LVT-lines can provide a comparatively cost-effective and visually unobtrusive means of noise reduction while maintaining the soft low-frequency response necessary for ground-borne vibration isolation.

Method

The track response is calculated using in-house software [8]. The waveguide finite element method (WFEM) is used for calculating the response of the free rail [9]. In WFEM, only the cross-section of a structure is discretized. Figure 3 shows the used FE-mesh of the rail. The solution of the WFE-problem consists of different

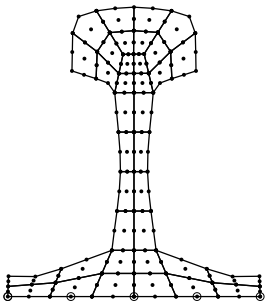

Figure 3: The discretized cross-section of the rail. Encircled nodes on the rail foot are used to couple the WFE model to the receptance of the support.

dispersive waves types, which are propagating and decaying along the length of the rail. Figure 4 shows the first six wave types found for a free UIC60 rail. A super-

Figure 4: Some wave types as calculated by the WFEM. From left to right: lateral bending, vertical bending, torsion, web bending (second order torsion), expansion, third-order torsion.

position of the different wave types allows the calculation of the point- and transfer-receptances necessary for calculating the TDR.

Yet, in most cases the rail is not free or continuously supported. A discrete support of the rail is realized by coupling the rail to an analytical receptance representing the slab, which is assumed rigid in the relevant frequency range, the elastic inlay described by its stiffness s_i, the sleeper mass m and the rail pad stiffness s_p, as shown in Figure 5 (a). The rail is connected to the sleepers at 119

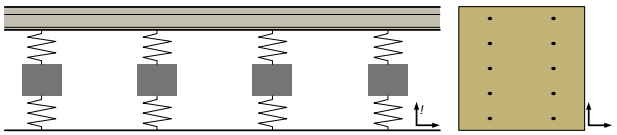

Figure 5: The continuous WFE rail is connected to an analytical receptance at each sleeper (a). At each sleeper, the receptance is represented by ten parallel springs arranged as shown in (b) to account for the spatial extend of the rail pad.

sleeper positions. This problem is solved in spatial domain, allowing a non-equidistant spacing of the support points [10, 7]. Using this, the rail pad is represented by ten parallel springs at each sleeper position. These are arranged in two lines of five springs each across the width of the rail as shown in Figure 5 (b). The total receptance below the foot of the rail at each sleeper can be described by the expression [3]

$$R = \frac{1}{s_p} + \frac{1}{s_i - \omega^2 m}. \qquad (1)$$

The equation shows that the response for low angular frequencies ω is determined mostly by the combined stiffness of the springs, and for high frequencies is determined mostly by the rail pad stiffness due to the increasing impedance of the mass. The two configurations are described in Table 1, and the corresponding receptances below the foot of the rail are shown in Figure 6. Damping is included as complex damping both in the rail and the support. The effective sleeper support stiffness in vertical direction (index v) is modelled as a series of the boot and the inlay elasticity,

$$s_{bi,v} = \frac{s_i s_b}{s_i + s_b}, \text{ with } s_i \ll s_b \;\rightarrow s_{bi,v} \approx s_i \qquad (2)$$

Table 1: Parameters for modelling the receptance below the rail.

Quantity	Unit	A	B
$s_{p,v}$	kN/mm	100	800
$s_{p,l}$	kN/mm	14	112
s_i	kN/mm	40	30
$s_{b,v}$	kN/mm	2000	2000
$s_{b,l}$	kN/mm	2000	2000
m	kg	99	99

which is mostly determined by the elastic inlay due to its significantly lower stiffness. The sleeper support stiffness in lateral direction (index l) remains unchanged between cases A and B, as the inlay only acts in vertical direction. From Figure 6 it is visible that the magnitude of the low-

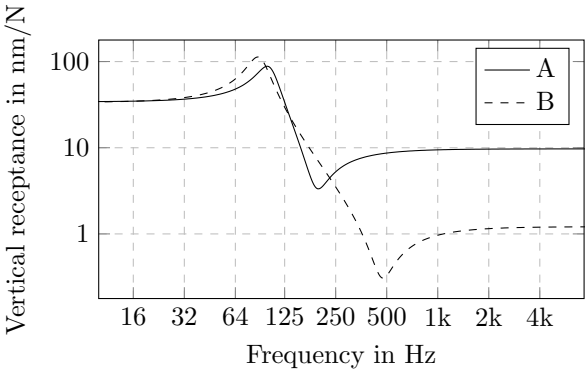

Figure 6: Comparison of the vertical track receptance below the foot of the rail for both setups.

frequency support stiffness is similar for both cases up to about 150 Hz, while the receptance is decreased by almost a magnitude above 300 Hz.

It should be noted that representing the response of the booted concrete block as a mass-spring-mass system is of course only an approximation, not taking into account the mounting position of the rail on the block, which is in reality not exactly centred, or the rail inclination. However, these construction specifications are here considered of minor importance for the vertical response of the system, especially at low frequencies due to the increasing decoupling between the rail and the concrete block with increasing frequency.

Results

The mid-span receptance on the head of the rail is shown in Figure 7 for both cases. Both responses show two highly damped resonances below 1000 Hz, corresponding to the in-phase and the 180° phase shifted motion of the sleepers and the rail. The first motion is mostly determined by the inlay stiffness, since the relative motion between the rail and the sleepers and thus the forces on the rail pad are comparatively small. The location of the first mode is therefore slightly lower for the lower inlay stiffness in case B at about 75 Hz compared to about 85 Hz for case A. The second mode is mostly determined by the rail pad stiffness and thus is significantly higher in case B

at around 600 Hz compared to 300 Hz for case A. The sharp resonances at around 1.1 kHz, 2.7 kHz and 5.3 kHz are a consequence of the interaction of the rail wave types with the discrete support. The peak at 1.1 kHz corresponds to the pinned-pinned mode, at which half a wavelength of the vertical bending wave corresponds to one sleeper span.

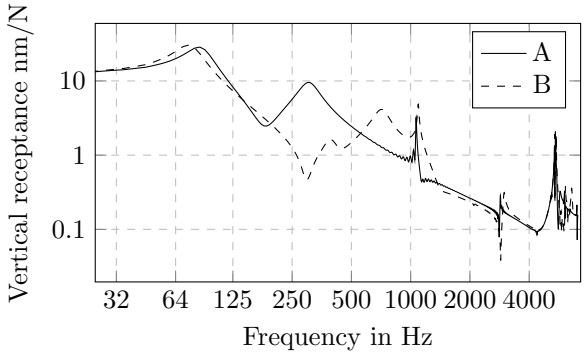

Figure 7: The vertical point receptance on the centre of the rail head.

The total vertical force on the rail pad closest to the excitation position is presented in Figure 8. In line with the reasoning above, we find a dip at the first mode and a high peak at the second mode for both cases. Above the second peak, case B shows a significantly higher force on the rail pad compared to case A, while the two cases are fairly similar towards low frequencies. Figure 9 shows the

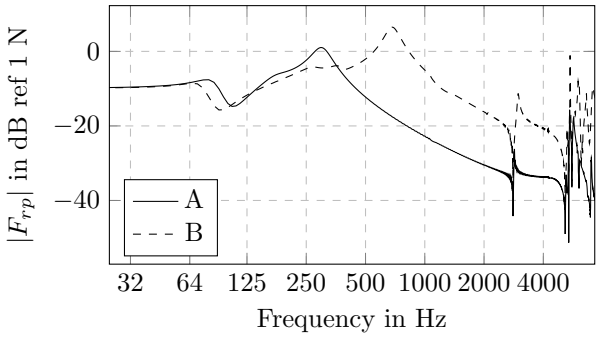

Figure 8: The vertical forces on the closest rail pad

receptance on the rail head in lateral direction. Case B shows a stiffer response at low frequencies as the changed elastic inlay only acts in vertical direction.

Finally, the track decay rates are presented in Figures 10 and 11. A significant increase in the vertical TDR above 250 Hz is found for case B in Figure 10. Since the relevant frequency range for radiation from rails is about 250 Hz to 3 kHz as seen in Figure 1, the increased track decay rate in this range is likely leading to a decrease in noise radiation. This is also supported by the fact that the TDR now lies much closer to or above the TSI limit curve. The lowered TDR below 250 Hz might relate to an increase in radiation from the rail, however, this is below the typical frequency range in which the rail is the dominant noise source. An increased TDR is also found

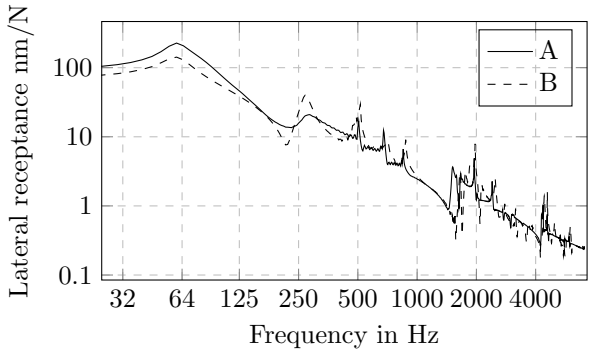

Figure 9: The lateral point receptance

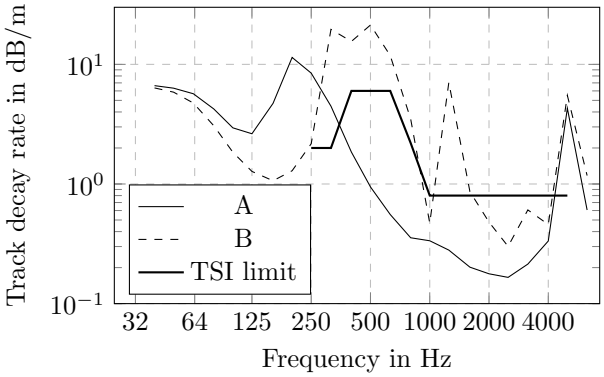

Figure 10: The vertical track decay rate.

in lateral direction, likely leading to a decreased noise radiation from the rail for similar excitation conditions.

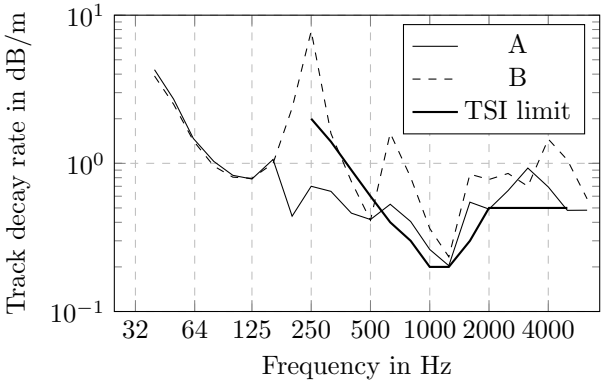

Figure 11: The lateral track decay rate.

Discussion

By increasing the rail pad stiffness and simultaneously decreasing the stiffness of the elastic inlay of low-vibration tracks, the low-frequency response can be maintained while the coupling between the rail and the sleeper can be increased significantly at high frequencies. It is known that an increased rail pad stiffness typically leads to a decreased noise radiation from the rail [3]. Higher forces between the rail and the sleeper above 400 Hz in case B can indicate an increase in the rolling contact forces. This needs to be further evaluated, as higher contact forces might develop an increased corrugation, thus

a higher roughness excitation and thereby a negative effect on the radiated noise. If necessary, this might need to be countered with more frequent rail grinding, leading to higher operating costs. Balancing this with the lower costs for implementation compared to other noise abatement measures such as noise barriers becomes an economic optimization task. However, the benefits of an easy to implement and visually unobtrusive solution might outweigh economic considerations in some situations. The actual difference in sound pressure level needs to be evaluated in further research. This is relevant, because an increased contact force might lead to higher radiation from the wheels and a stronger coupling between the rail and the sleepers might lead to a stronger radiation from the sleepers. Thus, the TDR is in this case not a sufficient predictor of the noise reduction. It is planned to quantify the total effect based on simulations and compare these to measurements of the Swiss railway operator SBB.

Conclusion

A comparatively simple modification of existing LVT track might lead to a reduction of the radiated noise from the track. The modification, exchanging the rail pads and boot inlays for stiffer and softer ones, respectively, leads to a stronger coupling between the sleeper and the rail and increases the rate at which the vibrations in the rail decay. This likely lowers the noise radiated from the rails. At the same time, the low-frequency response remains largely unchanged, preserving the low-vibration characteristics of the track. This modification might come at a cost of higher rolling contact forces, leading to higher wear on the rail. Quantifying this as well as the total effect of the noise reduction requires further research.

Acknowledgements

The current study is part of the ongoing activities in CHARMC – Chalmers Railway Mechanics (www.charmec.chalmers.se). Parts of the study have been funded from the European Union's Horizon 2020 research and innovation programme in the In2Track3 project under grant agreements No 101012456. The computations were performed on resources provided by the Swedish National Infrastructure for Computing (SNIC) at HPC2N. The valuable support from SBB is kindly acknowledged.

References

[1] S. R. Matias and P. A. Ferreira, "Railway slab track systems: review and research potentials," *Structure and Infrastructure Engineering*, vol. 16, pp. 1635–1653, Dec. 2020.

[2] P.-E. Gautier, "Slab track: Review of existing systems and optimization potentials including very high speed," *Construction and Building Materials*, vol. 92, pp. 9–15, Sept. 2015.

[3] D. J. Thompson, C. Jones, and P.-E. Gautier, *Railway noise and vibration: mechanisms, modelling and means of control*. Amsterdam ; Boston: Elsevier, 1st ed ed., 2009. OCLC: ocn245558640.

[4] X. Zhang, H. Jeong, D. Thompson, and G. Squicciarini, "The noise radiated by ballasted and slab tracks," *Applied Acoustics*, vol. 151, pp. 193–205, Aug. 2019.

[5] C. Jones, D. Thompson, and R. Diehl, "The use of decay rates to analyse the performance of railway track in rolling noise generation," *Journal of Sound and Vibration*, vol. 293, pp. 485–495, June 2006.

[6] B. Hemsworth, "REDUCING GROUNDBORNE VIBRATIONS: STATE-OF-THE-ART STUDY," *Journal of Sound and Vibration*, vol. 231, pp. 703–709, Mar. 2000.

[7] J. S. Theyssen, A. Pieringer, and W. Kropp, "The Influence of Track Parameters on the Sound Radiation from Slab Tracks," in *Noise and Vibration Mitigation for Rail Transportation Systems* (G. Degrande, G. Lombaert, D. Anderson, P. de Vos, P.-E. Gautier, M. Iida, J. T. Nelson, J. C. O. Nielsen, D. J. Thompson, T. Tielkes, and D. A. Towers, eds.), Notes on Numerical Fluid Mechanics and Multidisciplinary Design, (Cham), pp. 90–97, Springer International Publishing, 2021.

[8] J. S. Theyssen, E. Aggestam, S. Zhu, J. C. O. Nielsen, A. Pieringer, W. Kropp, and W. Zhai, "Calibration and validation of the dynamic response of two slab track models using data from a full-scale test rig," *Engineering Structures*, vol. 234, p. 111980, May 2021.

[9] C.-M. Nilsson, C. Jones, D. Thompson, and J. Ryue, "A waveguide finite element and boundary element approach to calculating the sound radiated by railway and tram rails," *Journal of Sound and Vibration*, vol. 321, pp. 813–836, Apr. 2009.

[10] X. Zhang, D. J. Thompson, Q. Li, D. Kostovasilis, M. G. Toward, G. Squicciarini, and J. Ryue, "A model of a discretely supported railway track based on a 2.5D finite element approach," *Journal of Sound and Vibration*, vol. 438, pp. 153–174, Jan. 2019.